Environmental Earth Sciences (2019) 78:122
https://doi.org/10.1007/s12665-019-8121-7

THEMATIC ISSUE

A case study on the height of a water-flow fracture zone above undersea mining: Sanshandao Gold Mine, China

Ying Chen[1] · Guoyan Zhao[1] · Shaofeng Wang[1] · Hao Wu[1] · Shaowei Wang[2]

Received: 7 October 2017 / Accepted: 4 February 2019 / Published online: 12 February 2019

Abstract

In undersea gold mines, the development of a water-flow fracture zone and its connection with the aquifer may cause massive water and sand inrush disasters. In this study, approaches including theoretical analysis, numerical simulation and field detection are employed to identify the development height of the water-flow fracture zone caused by undersea mining in the Xinli Zone of the Sanshandao Gold Mine to ensure mining safety. An improved Winkler elastic foundation beam model, considering the coupled influences of seawater pressure and backfill support, was established to calculate the height of the water-flow fracture zone. The result demonstrates that the height of the water-flow fracture zone depends on the elastic modulus of the overburden strata and the compression modulus of the filling material. Then, an experimental study utilizing a custom-made apparatus is conducted to obtain the Winkler foundation compression characteristics of the filling material used in the gold mining operation. The theoretical analyses are confirmed by numerical simulations and show that the height of the water-flow fracture zone decreases with the increase in mining level because the loads from overburden weight decreases with the mining depth. The theoretical analysis, numerical simulation and field detection present that the height of the mining-induced water-flow fracture zone is 39 m, 37 m, and 40.5–45 m, respectively, after mining at the − 135 m level. These values are reasonably consistent, suggesting that the proposed theoretical and numerical models and the utilized field detection method can provide valuable information for determining the overburden stability of an undersea mineral seam and improving mining safety.

Keywords Undersea mining · Winkle foundation model · Compression modulus · Water-flow fracture zone · UDEC · Digital borehole camera

Introduction

Mining underground may bring about collapse, harming the environment and causing fatalities and property loss (Huang et al. 2018a, b; Wang et al. 2008, 2018a). Underground mining usually causes strata movement; the strata above the excavation area will subside with different displacements and rates, resulting in separations between the fracture surfaces in those strata (Palchik 2003). The vertically adjacent strata will separate due to the differential displacements; then, fractures, called transverse fractures, will form parallel to the stratal planes. In the horizontal direction, the subsidence will cause the strata to break into rock blocks, which will rotate and separate, producing fractures, called longitudinal fractures, that are perpendicular to or intersect the stratal plane (Wang et al. 2017c). As the mining operation continues, the fractures will continue to develop upward. If the mining area is under a lake, river or sea, the fracture will become a channel and transport water (Hu et al. 2012). Once the water-flow fracture zone propagates to the bottom of the water zone, a disaster will occur (Zhao and Yan-Liang 2009). The mining-induced strata movement is influenced by strata and rock properties, mining performances, geostress

This article is a part of a Topical Collection in Environmental Earth Sciences on Water Resources and Hydraulic Engineering, guest edited by Drs. Yanqing Lian, Walton Kelly, and Fulin Li.

✉ Shaofeng Wang
wsfcumt@163.com; sf.wang@csu.edu.cn

Ying Chen
csu_chenying@csu.edu.cn

[1] School of Resources and Safety Engineering, Central South University, Changsha 410083, China

[2] Wenzhou Runxin Manufacturing Machine CO., Ltd, Wenzhou 325000, China

and geology conditions, etc. (Wang et al. 2016b, 2018b, c). Therefore, elucidating the development of the fractured zone in a timely manner is essential for the safe extraction of undersea deposits.

Considerable research has been conducted to forecast and monitor the height of water-flow fracture zones under various conditions (Booth 2006; Feldman et al. 2004; Yin et al. 2016; Zhang et al. 2012). To investigate the height of a water-flow fracture zone, theoretical analyses, numerical simulations and field detections have been adopted (Adhikary and Guo 2014; Booth and Bertsch 2002; Cherubini 2008; Zhang and Peng 2005). The multiple methods including empirical formula calculation, physical simulation and numerical simulation were used to forecast the evolution mechanism of water-flow fracture zones in shallow coal seams beneath a gully topography to ensure mining safety and groundwater protection (Wang et al. 2016a). Some theoretical mathematical models were proposed to determine the development of fractured zones (Hu et al. 2012). For example, a novel approach was proposed to quantify the relationship between the stratum separation and fracture evolution in undermined overburden; the theoretical distribution models of the void ratios of fractures were presented based on an analytical evaluation of the subsidence in the key strata (Wang and Li 2016; Wang et al. 2016b, 2017c). However, most of the previous studies focused on coal mining, and the theoretical mathematical models were usually established without considering the filling material.

Due to the complicated geographical conditions of underground or undersea mining, numerical simulations based on the finite element method (FEM) and discrete element method (DEM) can be used to forecast the development of the water-flow fracture zone caused by mining (Guo et al. 2017; Wang et al. 2017a; Ye et al. 2017; Zhang et al. 2017). Numerical simulations using Particle Flow Code (PFC) were conducted to detect the development height of the gas-conducting fracture zone in the overburden of coal seams, the results of which were confirmed by physical experiments on similar materials; it was verified that the temporospatial distribution characteristics of porosity could be used to forecast the height of the gas-conducting fracture zone and are of significant importance for determining the presence of a gas-conducting fracture zone (Wang et al. 2017b). In addition to the theoretical distribution models of the void ratios of fractures, a numerical model was established using the Universal Distinct Element Code (UDEC) and a sequence of image post-processing procedures (Wang and Li 2016; Wang et al. 2016b, 2017c). In addition, a numerical model using the three-dimensional Fast Lagrangian Analysis of Continua ($FLAC^{3D}$) software was established to forecast the height of the water-conducting fracture zone induced by longwall mining in shallow coal seams (Liu et al. 2015). In these numerical methods, the DEM-based methods, especially those that utilize UDECs, are by nature capable of simulating large and discontinuous displacements and fractures of undermined strata (Xu et al. 2016).

The Xinli Zone in the Sanshandao Gold Mine is the first subsea metal mine in China; the orebody is located tens to hundreds of meters under the sea. A permanent ore pillar that is several meters thick is used as the aquifer between the orebody and seawater; the in situ stress field is easily changed due to improper mining, which will induce potential hazards during the mining process (Peng et al. 2012).

Therefore, the analysis method to determine the height of the water-flow fracture zones should be different from the traditional method of coal mining. Far less research has been reported on the height of water-flow fracture zones induced by undersea mining, compared to those under other conditions. To protect the unique mining environment in the Xinli Zone and prevent water inrush disasters, thereby creating a safe and efficient mining environment, this study provides a comprehensive approach including theoretical analysis, numerical simulation and field detection to forecast and monitor the height of water-flow fracture zones in undersea mining.

Engineering background

The Sanshandao Gold Mine is located in the Sanshandao special industrial zone in Laizhou city, Shandong Province, China. The mining area is approximately 29 km north of Laizhou city and 45 km west of Zhaoyuan city. As shown in Fig. 1, it is located on the northeast coastline of Laizhou Bay. The Sanshandao Gold Mine (including the Xinli Zone and Xishan Zone) is a medium-sized underground mine (the production capacity of the Sanshandao Gold Mine is 8000 t/day) facing challenging mining environments. The main rock types surrounding the gold mine include metagabbro, monzogranite, and cataclastic rocks. In Xinli, the gold orebody extends from approximately − 40 m level to more than − 700 m under sea level. The orebody has a strike of NE 60°–70° and a dip angle of 40°–50° towards the southeast. To prevent seawater intrusion, an aquifer was assumed to be − 165 m above the orebody; the thickness of aquifer is approximately 115 m. The current mining depth is − 520 m. To maintain the stability of the undersea mining, the crown, sill and barrier pillars were retained in the mining process. Luckily, the seabed of the Xinli Zone at the Sanshandao Gold Mine is overlain by an approximately 2 ~ 3-m-thick gray silt soil and yellow silty clay layer. Scanning electron microscopy (SEM) studies on the microstructure of the subsea clay revealed that the pore connectivity in the clay is quite poor. The permeability of the clay is as low as 5–8 cm/s. This 2–3-m-thick clay layer serves as a nearly

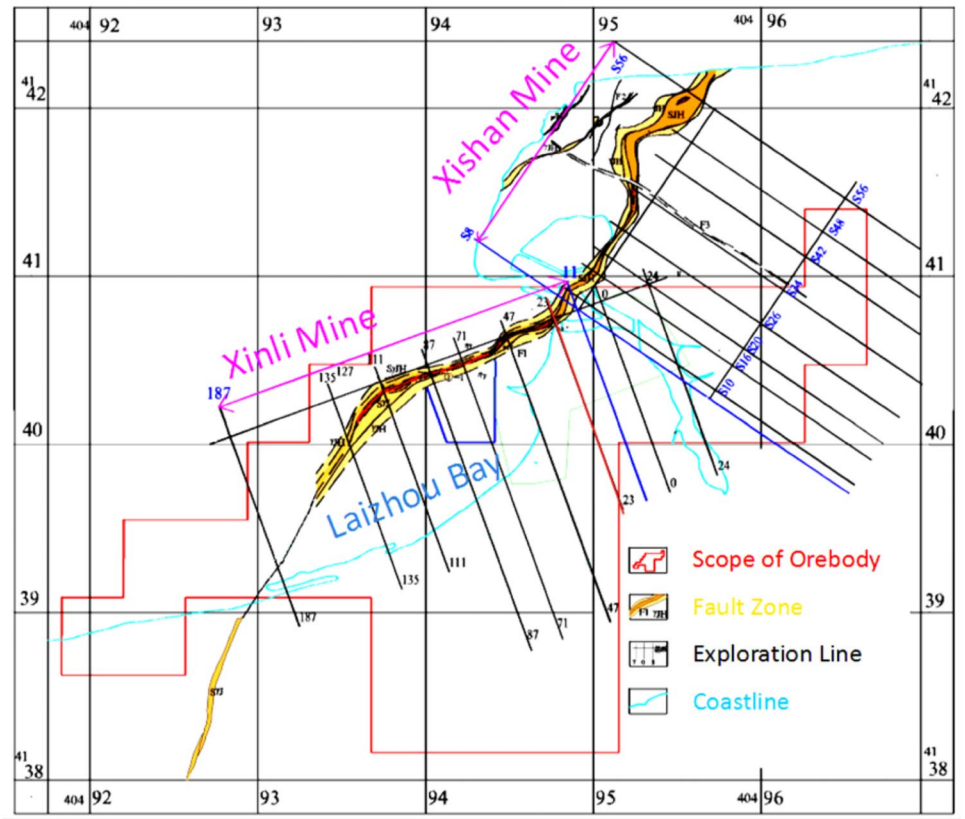

Fig. 1 The geologic map of the Xinli Zone at the Sanshandao Gold Mine

impermeable layer, inhibiting the seawater from infiltrating the seabed rock masses.

However, large mining disturbances may lead to an increase in the height of the water-flow fracture zone, which may connect with the aquifer. The increased height may lead to water inrush, threatening the undersea mining operation.

Theoretical analysis

The Winkler elastic foundation beam model

According to the cut-and-fill stoping method, filling materials must be added before the roof collapses. Compared with the open-stoping method and caving method, the deformation of the overlying rock is expressed as continuous bending; thus, a continuum mechanics analysis model can be established to analyze the stress in the strata. In the process of mining, except at both ends of the working face, the movement and deformation of the overlying rock along strike are the same. Therefore, this movement and deformation can be simplified as plane strain when analyzing the overlying rock in the middle of the stope. According to the rock characteristics, the filling and mining strata structure can be simplified as a laminated beam with elastic foundation, as is shown in Fig. 2.

As is shown in Fig. 3, the pressure from the overlying rock and seawater is regarded as the upper load, which is applied on the top of the support structure, and the filling material is regarded as the lower elastic support structure; thus, the single continuous elastic foundation beam model can be obtained.

Due to its symmetry, half of the model will be analyzed based on the Winkler elastic foundation beam theory, and the differential equation of the rock can be obtained as follows:

$$\mathrm{EI}\frac{\mathrm{d}^4 y}{\mathrm{d}x^4} + \frac{k}{\mathrm{EI}}y = \frac{q}{\mathrm{EI}}, \tag{1}$$

where *EI* is the bending stiffness of the rock, y is the deflection of the rock, k is the coefficient of the subgrade, and q is the loads from weights of overlying strata and seawater.

It should be noted that the value of the coefficient of the subgrade is important in this model. In surface or ground engineering, the subgrade is concrete or soil, but in underground mining, the subgrade is the filling material. Moreover, consolidation of the filling materials is a complex process. In general, fully consolidation process requires at least 3 months in undersea mining. Thus, during the consolidation time, the pressure from the overlying rock and seawater may lead to discontinuous movement,

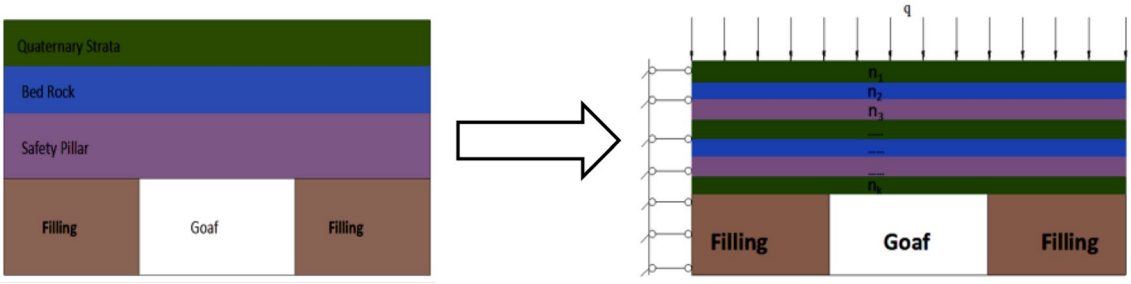

Fig. 2 The simplified model of the elastic foundation beam for overlaying strata in undersea mining

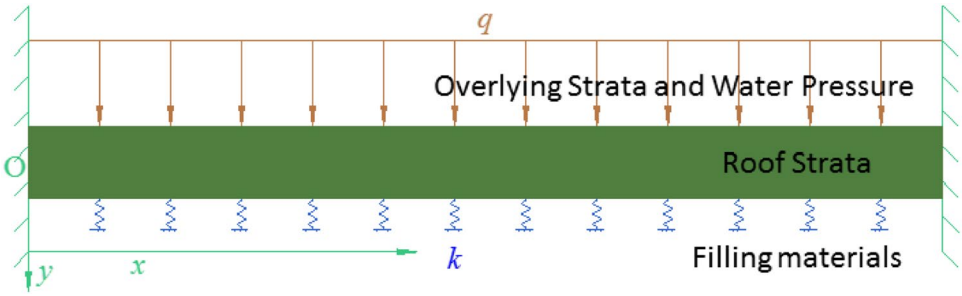

Fig. 3 The Winkler elastic foundation continuous beam for a single thin bedrock layer

deformation and fracturing in the roof. When the concentration of filling material is lower than 70%, it is regarded as a two-phase fluid (Sijing 2009). Therefore, the deformation coefficient of the filling material can be expressed as $k=\frac{E_t l^4}{\mathrm{EI}}$, where E_t is the compression modulus of the filling materials, and l is the length of the beam (Ghavanloo et al. 2010).

The general solution of Eq. (1) can be obtained as follows:

$$y = e^{\alpha x}(A\cos\alpha x + B\sin\alpha x) + e^{-\alpha x}(C\cos\alpha x + D\sin\alpha x) + \frac{q}{k}. \tag{2}$$

According to the boundary conditions, the deflection equation of the overlying rock can be obtained as follows:

$$y = \frac{2q}{k}\cdot\frac{\sinh(2l\alpha)-\sin(2l\alpha)}{\sinh(2l\alpha)+\sin(2l\alpha)}\cdot\beta_1 - \frac{q}{k}\cdot\frac{\cosh(2l\alpha)-\cos(2l\alpha)}{\cosh(2l\alpha)+\cos(2l\alpha)}\cdot\beta_{2+}\frac{q(1-\beta_3)}{k}, \tag{3}$$

where l is the length of the overlying rock, $\alpha = \sqrt[4]{k/4\mathrm{EI}}$, $\beta_1 = \sinh\alpha x\sin\beta x$, $\beta_2 = \frac{1}{4}(\cosh\alpha x\sin\alpha x - \sinh\alpha x\cos\alpha x)$, and $\beta_3 = \cosh\alpha x\cos\alpha x$.

According to elastic mechanics, the deflection of the overlying rock can be obtained as follows:

$$M(x) = -\mathrm{EI}\frac{\mathrm{d}^2 y}{\mathrm{d}x^2}. \tag{4}$$

The inertia moment of the overlying rock is $I_z = \frac{H^3}{12}$, where H represents the thickness of overlying rock, and the normal stress of the arbitrary point in the overlying rock is as follows:

$$\sigma = \frac{M(x)H_t'}{I_z} = \frac{12M(x)H_t'}{H^3}, \tag{5}$$

where H_t' is the height between the arbitrary point and the neutral plane of the overlying rock.

Assume that the rock will crack if the normal stress σ reaches the tensile strength σ_t:

$$\sigma = \frac{12M(x)H_t'}{H^3} = \sigma_t. \tag{6}$$

By combining Eqs. (3, 5) and (6), the relationship between E_t (the compression modulus of the filling materials) and H_f' (the height of the water-flow fracture zone) can be obtained as follows:

Fig. 4 Laser diffraction particle size analyzer

$$\begin{cases} H_{\mathrm{t}}' = \frac{\sigma_t E_t l^4}{\alpha^2 qTE} \\ H_{\mathrm{f}}' = \frac{n}{2} - H_t' = \frac{n}{2} - \frac{\sigma_t E_t l^4}{\alpha^2 qTE} \\ T = A\cos\alpha x\cosh\alpha x + B(\sin\alpha x\cosh\alpha x + \cos\alpha x\sinh\alpha x) - 2\sin\alpha x\sinh\alpha x \cdot \\ A = 4\frac{\sinh(2l\alpha)-\sin(2l\alpha)}{\sinh(2l\alpha)+\sin(2l\alpha)} \\ B = \frac{\cosh(2l\alpha)-\cos(2l\alpha)}{2\cosh(2l\alpha)+\cos(2l\alpha)} \end{cases} \tag{7}$$

where n is the thickness of beam composed of overlying strata. The above equation proves that the height of a water-flow fracture zone depends on not only the elastic modulus of the overlying rock, but also the compression modulus of the filling materials. The elastic modulus of the overlying rock depends on the physical and mechanical properties of the rock, while the compression modulus of the filling materials depends on the compression characteristics of the filling materials.

The mechanical analyses mentioned above prove that the height of a water-flow fracture zone has a relationship with the compression modulus of the filling materials. Tailing are used as the main filling materials in the Xinli Zone. After filling in the stope, the normal stress from the roof increases with the settlement of the overlying rock; the filling materials will be compressed, and the compression modulus will increase. To determine an accurate prediction of the height of the water-flow fracture zone, it is necessary to conduct an experiment to determine the compression characteristics of the filling materials.

The compression experiment of the backfill material

Properties of backfill materials

The properties of the backfill materials had been obtained, before the compression experiment. The backfill materials include the tailings and a cementitious material called C material. The test items include moisture content, specific density, bulk density, permeability coefficient, porosity, the distribution of particle size, and chemical composition.

The tailings were divided into five groups, which were put in the drying box first. Then, the density pycnometer, Kamenski tube, X-ray diffractometer, and laser diffraction particle size analyzer (Fig. 4) were used to perform the tests for the tailings. The results are listed in Tables 1 and 2. The distribution curve

Table 1 The test results of the tailings

No.	Moisture content (%)	Specific density (g/cm^3)	Bulk density (10^3 kg/m^3)	Permeability coefficient (cm/h)	Porosity (%)
1	2.20	2.57	1.372	13.97	46.39
2	2.10	2.59	1.402	14.14	47.12
3	2.12	2.50	1.370	14.01	46.59
4	2.14	2.53	1.345	14.05	46.43
5	2.09	2.54	1.346	14.03	46.97
Average	2.13	2.55	1.359	14.04	46.70
Difference rate	5.1%	3.5%	4.2%	1.2%	1.5%

Table 2 The main components of the tailings (mass fraction of metal element)

Metal element	Al	Fe	K	Ca	Na	Mn	Pt	Zn	Cu
Content (%)	3.79	1.21	1.94	0.58	0.18	0.08	0.04	0.04	0.03

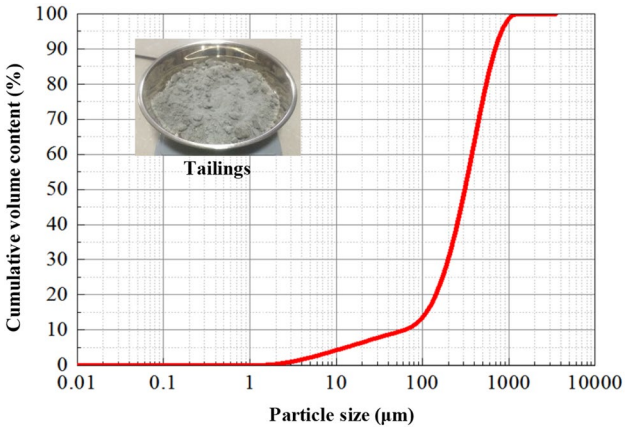

Fig. 5 The distribution curve of particle size in tailings

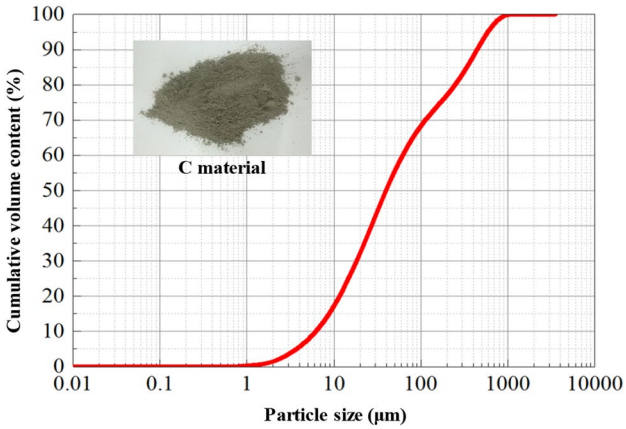

Fig. 6 The distribution curve of particle size in C material

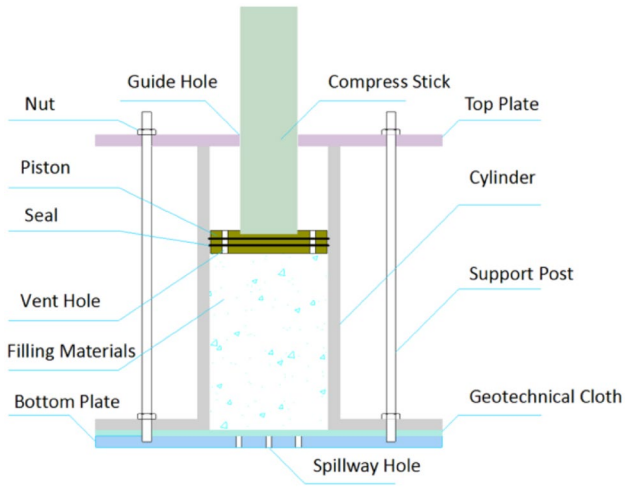

Fig. 7 Compression box

of the particle size in tailings and C material are shown in Figs. 5 and 6, respectively. The results show that the tailings and C material present a uniform particle size distribution and an excellent gradation continuity, which can ensure a good consistency among the filling samples in experiments.

Experimental apparatus

A compression box was designed for holding and compressing filling materials and is presented in Fig. 7. The box includes a top plate, bottom plate, cylinder, compress stick, piston and support post. The materials for these components must have a hardness, stiffness and wear resistance that meet the experimental requirements. Based on the characteristics of the apparatus, radial and circumferential deformation can be ignored during the compression experiment. To minimize frictional resistance between the cylinder and the filling materials, the inner wall of the cylinder and the compress stick must be polished and anointed before the experiment. The vent hole on the top plate was used to control the rate of pressure application. The bottom plate was equipped with a spillway hole, which can be closed or opened to allow different drainage conditions (undrained to fully drained) during the compression experiment. A geotechnical cloth was laid on the bottom plate to avoid the loss of tailings as the water flowed through the spillway hole.

A computer-controlled electro-hydraulic servo universal testing machine shown in Fig. 8a was used to compress the filling materials, while a full digital high-response measurement system was used to monitor the changes in displacement, load and time, which can be seen in Fig. 8b. The experimental control mode adopts load control, according to the magnitude of the deep ground stress, the target load was 259.77 kN (30 MPa), and the loading speed was 4 kN/s (approximately 0.5 MPa/s). Each test included three experiments, and the results were averaged.

The experimental results

The confined compression experiment of the filling materials was carried out to determine the compressive deformation characteristics of the cementitious filling materials. The filling height of the tailings is 210 mm, and the tailings are slightly vibrated during loading to reduce the error caused by the formation of artificial pores. The compression rate is used to characterize the compression characteristics of the filling materials. The compression ratio is calculated according to the following equation:

$$\varepsilon = \frac{\Delta h}{h} \times 100\%, \tag{8}$$

where ε is the compression rate; Δh is the axial compression amount; and h is the uniform height of the filling material and is 210 mm.

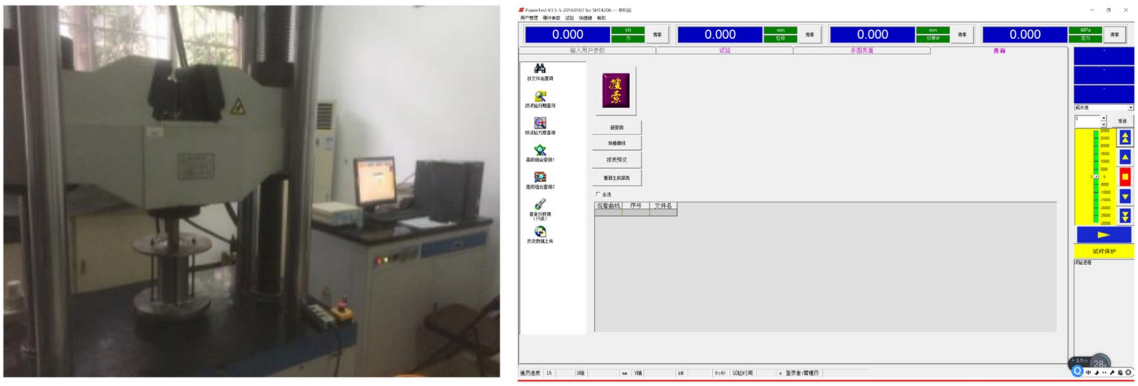

Fig. 8 Compression test system for filling materials. **a** the universal testing machine, **b** the response system

Table 3 Conditions of the compression tests of filling materials

No.	Density (g/cm^3) (before compress)	Content ratio of C material (%)	Moisture content (%)	Consolidation time (h)	Density(g/cm^3) (after compress)	ε (%)
1	2.56	12	6	0	2.32	33.07
2	2.47	8	12	12	2.41	26.53
3	2.62	4	3	8	2.39	31.75
4	2.52	4	9	20	2.36	30.19
5	2.42	6	15	2	2.29	30.24
6	2.67	10	0	24	2.73	20.13
7	2.67	8	0	4	2.74	19.73
8	2.47	10	12	10	2.48	23.90
9	2.41	12	15	72	2.56	18.63
10	2.51	14	9	6	2.38	28.96
11	2.61	14	3	16	2.45	29.04
12	2.57	6	6	168	2.40	30.00

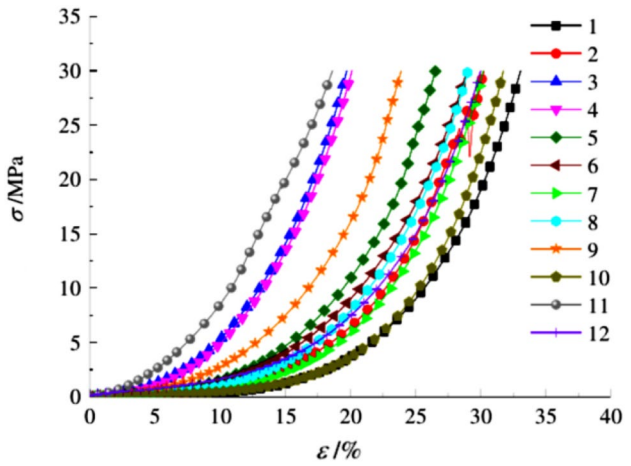

Fig. 9 Compression curves of filling materials under different test conditions

The test conditions and associated results are shown in Table 3 and Fig. 9, respectively.

Under the condition of complete confinement, the ratio of the vertical pressure to the strain increment is the compression modulus (Zhao and Bai 2009; Jehring and Bareither 2016). Therefore, the compression modulus of the filling materials can be expressed as follows:

$$E_t = \frac{\sigma_1 - \sigma_0}{\varepsilon_1 - \varepsilon_0}, \tag{9}$$

where ε_1 and ε_0 are the compression ratios of the filling body, and σ_1 and σ_0 are the corresponding stresses.

Based on the experiment results and the Eq. (9), the compression modulus of the filling materials used in undersea mines can be gotten, and then the compression modulus can be used as an essential parameter to calculate the height of

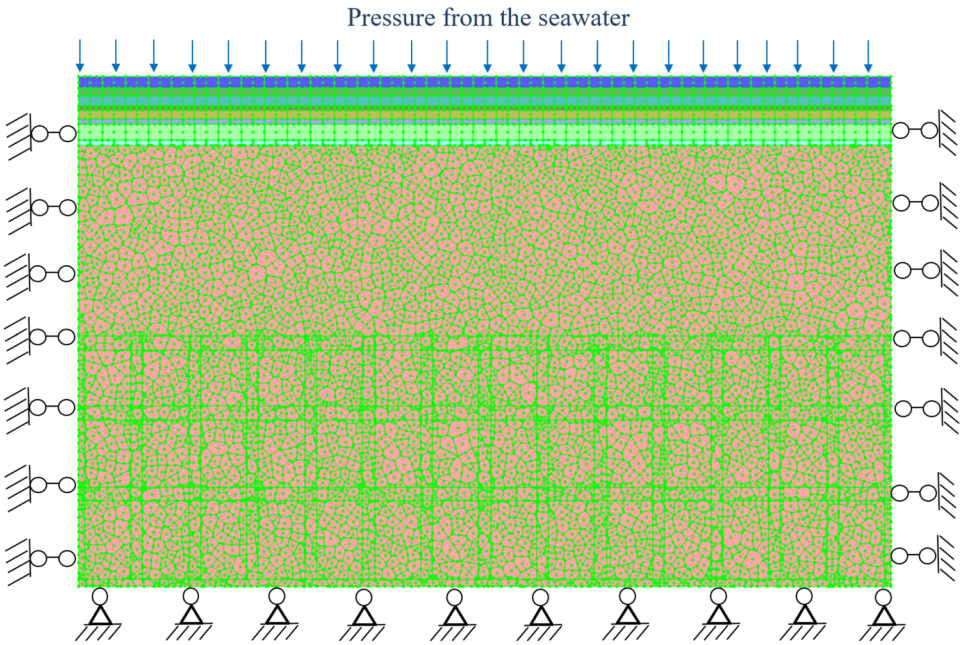

Fig. 10 UDEC model for the numerical simulation of undermining-induced fractures

the water-flow fracture zones in the Xinli Zone based on Eq. (7). The result can be seen in Table 6.

The numerical simulation

The UDEC was adopted to analyze the evolution of the fractures in the overlying strata in this undersea mining area. The dimension of the model is represented by a length × height of 220 × 350 m. The failure criterion used in the numerical analyses is the Mohr–Coulomb model. As shown in Fig. 10, the model is subjected to the following boundary conditions: horizontal displacement boundary conditions are applied to left and right sides; a stress boundary condition is applied to the top; horizontal and vertical displacement boundary conditions are applied to the bottom; and an in situ stress boundary condition is applied in a stepwise manner to match the stress distribution with the actual in situ stress. The mechanical parameters of the rock blocks and rock contacts in the models are shown in Tables 4 and 5, respectively. The geomechanical parameters used in the numerical model were achieved by performing conventional triaxial compression tests and direct shear/tension tests of intact rock samples

Table 4 The main ground parameters in the Xinli Zone

Lithology	Depth (m)	Density (kg/m^3)	Elastic modulus (GPa)	Poisson's ratio	Tensile strength (MPa)	Cohesion (MPa)	Internal friction angle (°)
Weathered sandstone	4.2	1800	3.44	0.2	1.35	0.35	30.6
Gritstone	5.2	2420	4.02	0.19	1.23	0.45	32.6
Sand-shale 1	7.5	2230	3.1	0.24	1.15	0.18	36.94
Mudstone	8.6	2520	9.8	0.19	1.08	0.25	38.7
Siltstone	12.7	2620	2.24	0.2	1.20	0.38	30.6
Sand-shale 3	13.5	2510	3.08	0.19	1.45	0.26	32.6
Medium sandstone	14.7	2600	1.19	0.24	1.05	0.30	36.94
Sand-shale 2	18.5	2570	2.3	0.19	1.17	0.22	38.7
Medium sandstone	20.7	2540	2.28	0.19	1.34	0.21	32.6
Siltstone	27.6	2635	2.29	0.24	1.24	0.38	36.94
Fine sandstone	30	2450	1.20	0.19	1.26	0.45	38.7
Orebody	–	2709	3.48	0.19	0.60	0.50	32.0
Floor rock	–	2640	5.30	0.24	1.06	0.88	35

Table 5 Contact properties used in the numerical simulation

Contact	Normal stiffness (GPa/m)	Shear stiffness (GPa/m)	Tensile strength (MPa)	Cohesion (MPa)	Friction angle (°)
Weathered gritstone	32.4	10.52	0.87	2.19	19.72
Gritstone-sand-shale 1	26.7	8.90	0.91	2.04	19.3
Sand-shale 1-mudstone	16.3	6.19	0.55	1.82	15.63
Mudstone-siltstone	10.21	3.77	0.43	1.03	12.79
Siltstone-sand-shale 2	18.24	7.12	0.54	2.38	16.08
Sand-shale 2-medium sandstone	13.25	4.98	0.49	1.425	14.21
Medium sandstone-sand-shale 3	18.69	6.23	0.64	1.43	13.51
Sand-shale 3-medium sandstone	13.25	4.98	0.49	1.425	14.21
Medium sandstone-siltstone	18.14	5.89	0.49	1.23	11.04
Siltstone-fine sandstone	10.89	3.53	0.29	0.74	6.63
Fine sandstone-rock	25.92	8.42	0.70	1.75	15.78
Rock-orebody	21.36	7.12	0.73	1.63	15.44
Voronoi-based joint in orebody	31.40	10.82	0.92	2.245	19.51

extracted from the geological exploration boreholes (Sanshandao Gold Mine 2012). Accounting for the fact that the behaviors of a rock block and a rock joint at the scale of a core differ significantly with the behaviors at the mine scale, the overall geomechanical behavior of the strata in the model was determined by strength reduction and changing the density of the Voronoi-based joints to ensure that the strata subsidence obtained in numerical simulation has a reasonable agreement with the field strata displacement measuring.

Based on the actual mining process, the simulation model was established with three mining stages: the − 240 m level (from − 240 m depth to − 200 m depth), − 200 m level (from − 200 m depth to − 165 m depth) and − 165 m level (from − 165 m depth to − 135 m depth). The overlying and underlying strata are affected during mining. Fractures separating the strata along strata planes and those crossing the strata connect, forming a variable water-flow fracture zone. This disturbance may lead to the subsidence, vertical displacement and shear failure of the strata. Then, the primary fractures in the rock will crack along the existing joint surfaces, creating new fractures. The abundant new fractures will lead to the continuous development of a water-flow

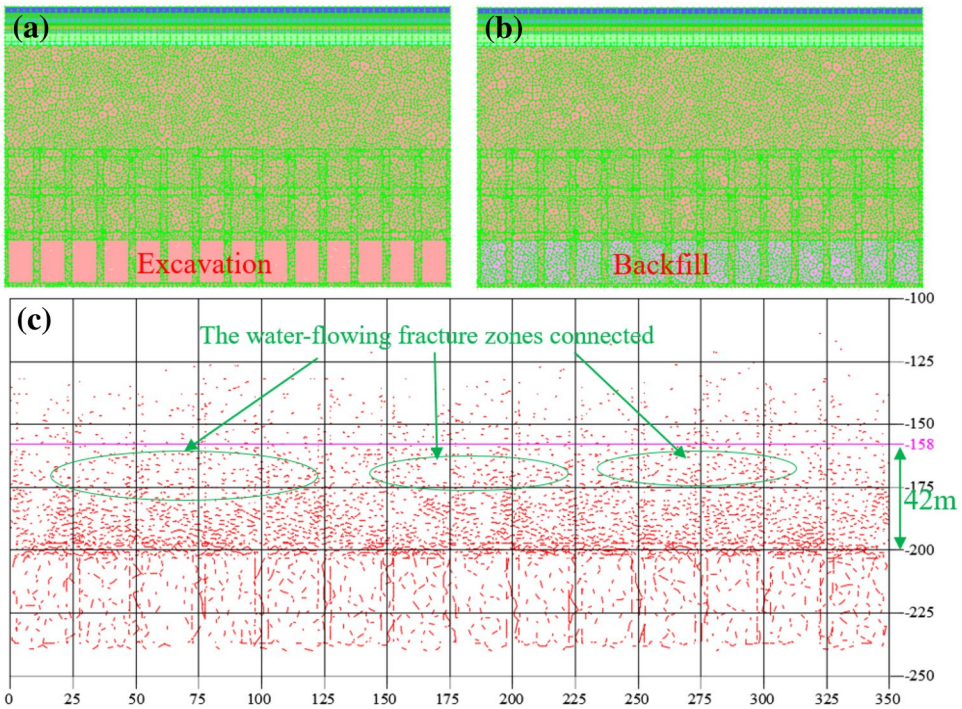

Fig. 11 Height of the fracture zone during mining at the − 240 m level: **a** excavation and **b** backfill of the stope in the − 240 m level and **c** open fractures

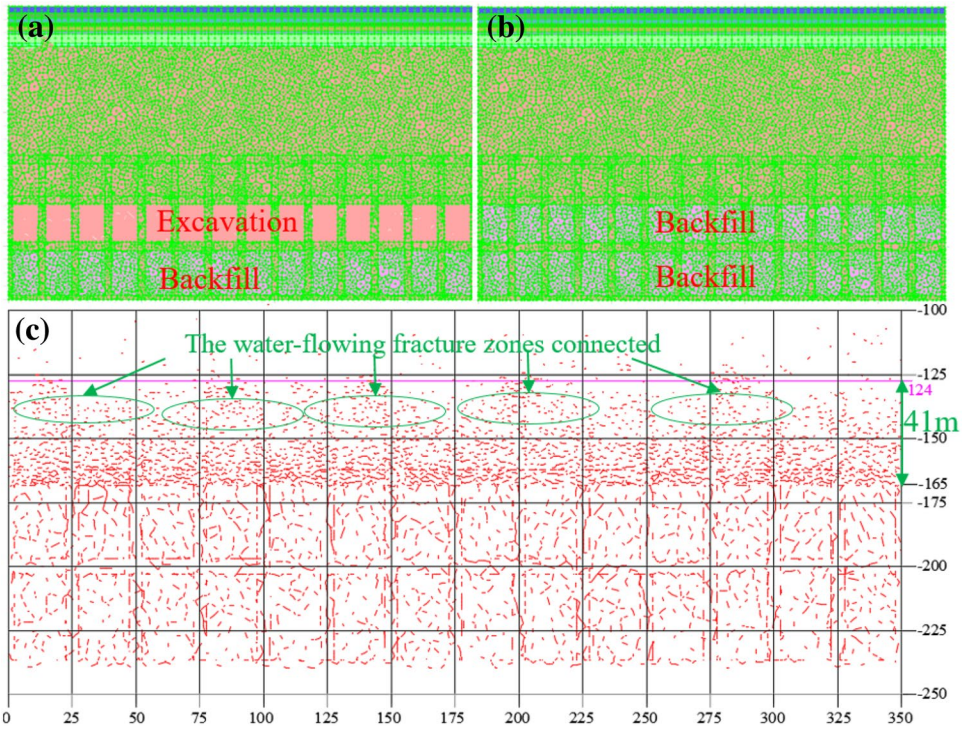

Fig. 12 Height of the fracture zone during mining at the − 200 m level: **a** excavation and **b** backfill of the stope in the − 200 m level and **c** open fractures

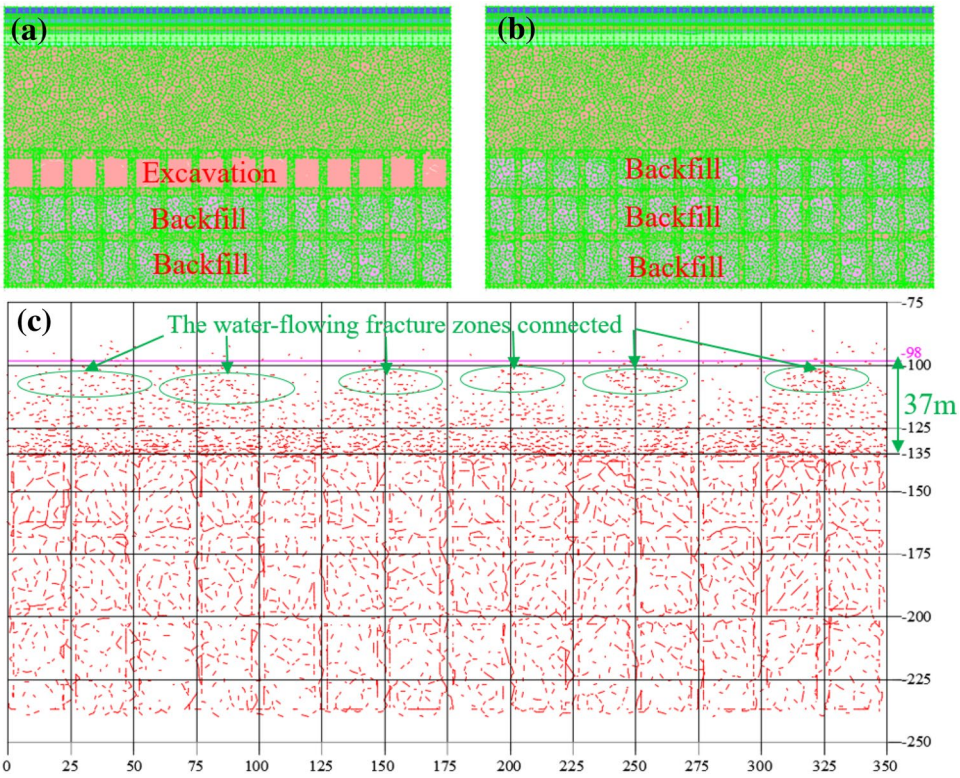

Fig. 13 Height of the fracture zone during mining at − 165 m level: **a** excavation and **b** backfill of the stope in the − 165 m level and **c** open fractures

fracture zone. The field survey provided the direction and length of the joints in the Xinli Zone, which are discrete, so the simulation adopted the Voronoi-based method to discretize the rock and create a discrete fracture network in the numerical simulation.

Based on the numerical analyses, the development of water-flow fracture zones can be observed in Figs. 11, 12

Fig. 14 The digital borehole camera

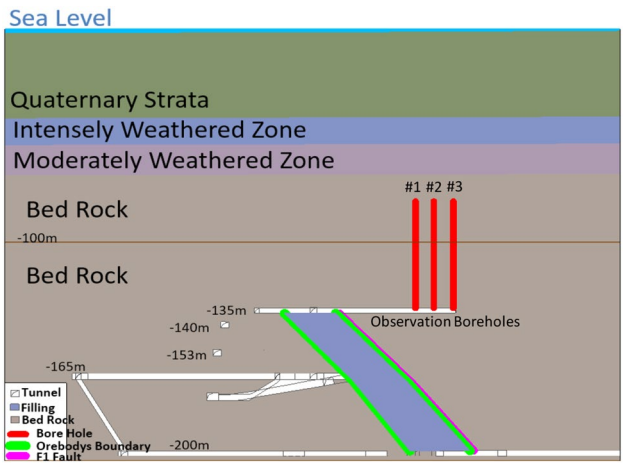

Fig. 15 The design of the observation borehole

and 13. The results show that the fractures in the rock propagate upward gradually with the excavation of orebody. When mining at the − 240 m level, it was clear that many of the preexisting fractures propagated to the − 200 to − 175 m height, and the fracture development was intensive and created high connectivity, proving that the water-flow fracture zone had crossed this height and developed upward. At the height of − 175 to − 125 m, the number of cracks was small, the degree of development was low, and the connectivity was weak. By observing the intensity of fracture development, it was found that the water-flow fracture zone had developed to − 158 m and that the height of the water-flow fracture zone was 42 m. With continued mining to the − 200 m level, the water-flow fracture zone developed to a height of − 124 m, and the height of the water-flow fracture zone was 41 m. During mining at the − 165 m level, the water-flow fracture zone developed to − 98 m, and the height of the water-flow fracture zone was 37 m. The fractured zone has not yet reached the seabed.

Field detection

The height of the water-flow fracture zone was detected by the digital borehole camera shown in Fig. 14. The rock formation images inside the hole can be clearly and directly shown on a computer shot by the digital borehole camera (Cao et al. 2015). The location of fracture zone can be visually observed from borehole images, and the results can be used to verify the accuracies of the theoretical analysis and numerical simulation.

As shown in Fig. 15, the three boreholes were drilled at the − 135 m level into the overlying strata to observe the strata fracturing during the excavation of the − 165 m level. The diameter of each borehole is 75 mm, the length is 50 m, and the orientation is vertical. The results of the field detection are shown in Figs. 16, 17 and 18.

By comparing and analyzing the observation results from the three different boreholes, the following can be concluded:

(a) The #1 borehole result shows that below 46.0 m, the density of the fractures is greater than above 46.0 m, and most of the fractures connect with each other. Above 46.0 m, the fracture density decreases, and the connectivity of fracture also decreases.
(b) The #2 borehole result shows that below 45.0 m, the density of the fractures is greater than that above 45.0 m, and most of the fractures are connected with each other. Clearly, the integrity of this range is very bad. Above 45.0 m, the fracture density and associated connectivity decrease, which indicates that the integrity of this rock is better than that below 45.0 m.
(c) The #3 borehole result shows that there are abundant fractures on the borehole wall below 40.5 m, and most of the fractures are connected with each other. Above 40.5 m, the density and connectivity of fractures decrease.
(d) From the results of the three boreholes, the following can be concluded: the height of the water-flow fracture zone at the − 135 m level induced by the excavation of the − 165 m level is 40.5–45.0 m.

Results and discussion

The work mentioned above analyzed the development of a fractured zone above undersea mining. According to the empirical formula from the National Bureau of Coal Industry of China, the Xinli Zone can be regarded as a medium

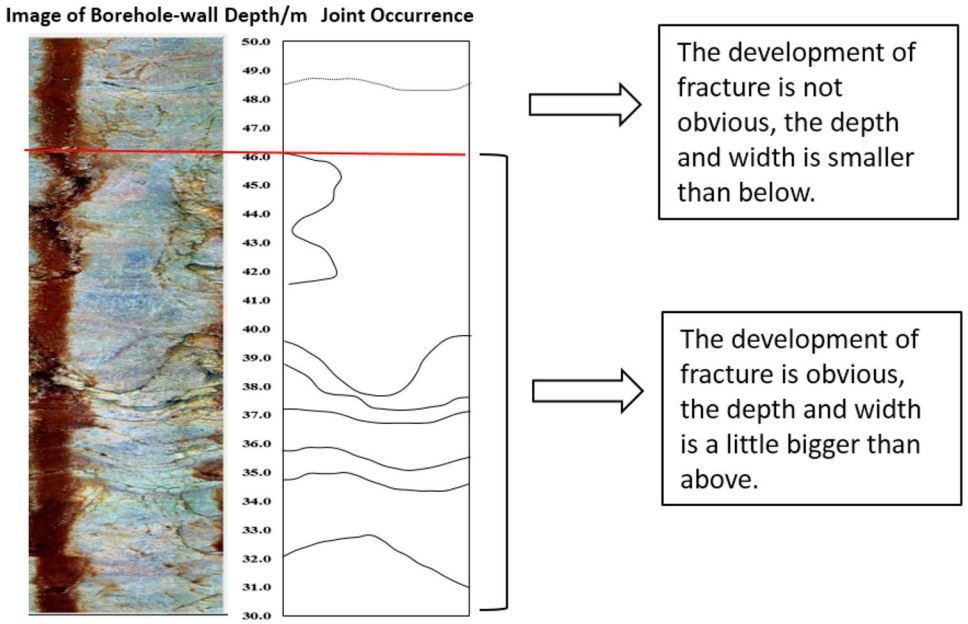

Fig. 16 The image of borehole #1

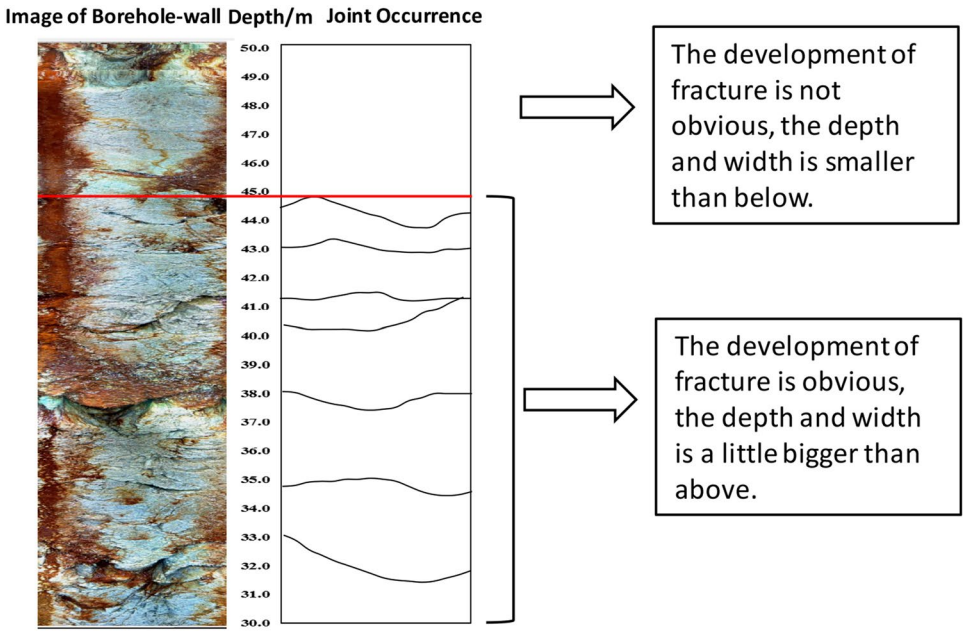

Fig. 17 The image of borehole #2

hard rock, and the empirical formula of the height of the water-flow fracture zone in overlying strata above mined-out area can be described as (State Bureau of Coal Industry 2000):

$$H_{\mathrm{d}} = \frac{100 \sum M}{1.6 \sum M + 3.6} \pm 5.6, \tag{10}$$

where H_{d} is the height of the water-flow fracture zone; and $\sum M$ is the cumulative mining height.

In this study, theoretical analysis, numerical simulation and field detection are used to forecast the evolution height of a water-flow fracture zone above undersea mining. To consider the filling materials in the Xinli Zone, the result from the No. 8 test can be selected and substituted in Eq. (7). Then, the height of the water-flow fracture zone during mining at the − 165 m level can be calculated, and the results obtained by theoretical analysis, numerical simulation, empirical formula and field detection are shown in Table 6.

In comparing the four results, the results from the theoretical analysis, numerical simulation and field detection are

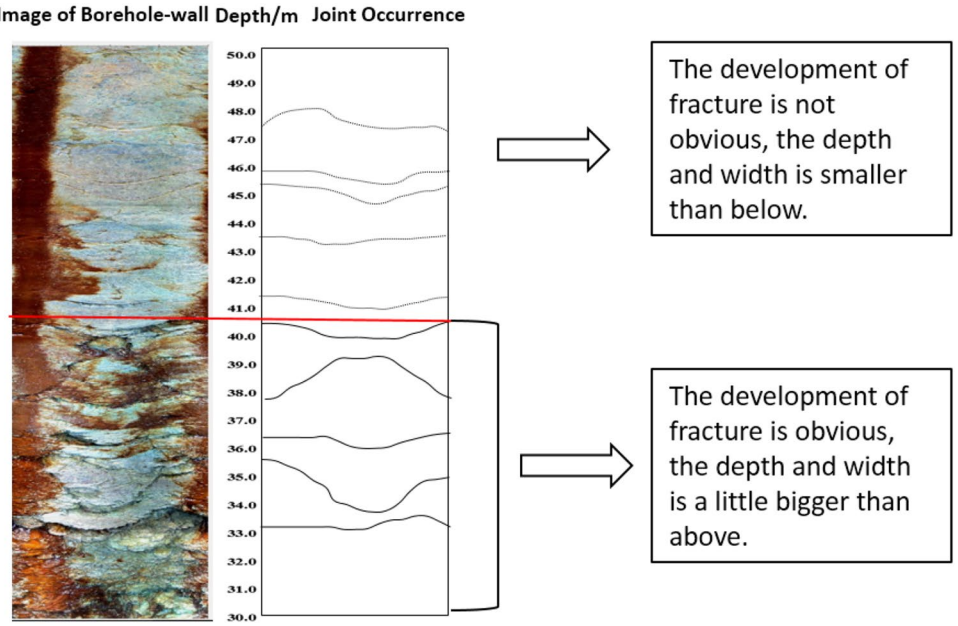

Fig. 18 The image of borehole #3

Table 6 Results of the height of the water-flow fracture zone

Theoretical analysis	Numerical simulation	Empirical formula	Field detection
39 m	37 m	46.4–57.6 m	40.5–45 m

similar, indicating that the improved Winkler foundation model can be used more successfully to forecast the height of the water-flow fracture zone above undersea mining compared with the empirical formula used in coal mining. The height obtained by the UDEC numerical simulation is 37 m, which is very close to the value obtained by the theoretical analysis and field detection. This verification proved that the porosity parameters derived from the UDEC numerical simulation produce a valuable reference for the water-flow fracture zone height prediction. The result from the empirical formula from coal mining is slightly higher than the other three results, indicating that the empirical formula is slightly inaccurate and not suitable for undersea mining. In addition, the accuracy of the derived formula based on the Winkler foundation model has been confirmed by results of the numerical simulation and field detection. Therefore, the proposed model expressed as Eq. (7) can be selected by a mining engineer to predict the height of a water-flow fracture zone induced by undersea mining and to provide a valuable reference for determining the extent of the impermeable rock mass between the seabed and mining face to prevent seawater inrush and improve mining safety.

Conclusions

The height of a water-flow fracture zone in mining-disturbed overlying strata is of great importance for prevention of water inrush disasters, particularly in undersea mining. This study performed a case study to investigate the height of the water-flow fracture zone above the Xinli Zone undersea mining operation, using a method that combined theoretical analysis, DEM-based numerical simulation and field detection. From this study, the following conclusions can be drawn.

(a) A theoretical model based on the Winkler foundation model was established to calculate the development height of the water-flow fracture zone, considering the seawater pressure and backfill support. The model shows that the height of the undermining-induced water-flow fracture zone is correlated with the deformation and strength parameters of the overlying rock, the compression modulus of the backfill material, the size of the mined-out area and the loads from the seawater and overlying strata. Therefore, improving the compressive capacity and compaction degree of the backfill material and decreasing the mined-out scale are effective measures for decreasing the height of the water-flow fracture zone to prevent seawater inrush hazard and increase the upper limit of mining; thus, more undersea gold resources can be safely mined.

(b) The DEM-based numerical model was established using UDEC software and a Voronoi-based joint network to simulate the height of the water-flow fracture zone induced by excavation and backfill at different

mining levels. The results show that the height of the fractured zone during mining at the levels of − 240 m, − 200 m and − 165 m are 42 m, 41 m and 37 m, respectively. The height of the water-flow fracture zone decreases with the increase in mining level because the loads from the overburden weight decrease as the mining depth decreases, which agrees with the conclusion drawn from the theoretical model.

(c) During mining at the − 165 m level, the heights of the mining-induced water-flow fracture zones determined by theoretical analysis, numerical simulation and field detection are 39 m, 37 m, and 40.5–45 m, respectively. These values are reasonably consistent, compared to the result of 46.4–57.6 m calculated by the empirical formula used in coal mining. The results indicate that the empirical formula of the height of a coal mining-induced fracture zone is not suitable for use in undersea mining of gold resources in hard rock. Instead of this empirical formula, the proposed theoretical model can be adopted by a mining engineer to predict the height of a water-flow fracture zone induced by undersea mining, and the accuracy of this model has been confirmed by the results of a numerical simulation using UDEC and the results of field detection using a digital borehole camera. Therefore, the proposed theoretical and numerical models and the utilized field detection method can provide a valuable reference for determining the impermeability of the strata overlying an undersea mineral seam, between the seabed and mining face, to prevent seawater inrush, enable undersea mineral resources to be mined and improve mining safety.

Acknowledgements The project is sponsored by the National Natural Science Foundation of China (Nos. 51774321 and 51804163) and the National Key R&D Program of China (2018YFC0604606). The authors would like to thank those at the Sanshandao Gold Mine who provided considerable support during field detection and data collection.

References

Adhikary DP, Guo H (2014) Measurement of longwall mining induced strata permeability. Geotech Geol Eng 32:617–626. https://doi.org/10.1007/s10706-014-9737-8

Booth CJ (2006) Groundwater as an environmental constraint of longwall coal mining. Environ Geol 49:796–803. https://doi.org/10.1007/s00254-006-0173-9

Booth CJ, Bertsch LP (2002) Groundwater geochemistry in shallow aquifers above longwall mines in Illinois, USA. Hydrogeol J 7:561–575. https://doi.org/10.1007/s100400050229

Cao Y-B, Feng X-T, Yan EC, Chen G, Lü F-f, Ji H-b, Song K-Y (2015) Calculation method and distribution characteristics of fracture hydraulic aperture from field experiments in fractured granite area. Rock Mech Rock Eng 49:1629–1647. https://doi.org/10.1007/s00603-015-0881-0

Cherubini C (2008) A modeling approach for the study of contamination in a fractured aquifer. Geotech Geol Eng 26:519–533. https://doi.org/10.1007/s10706-008-9186-3

Feldman WC, Head JW, Maurice S, Prettyman T, Elphic RC, Funsten HO, Lawrence DJ, Tokar R, Vaniman D (2004) Recharge mechanism of near-equatorial hydrogen on Mars: Atmospheric redistribution or sub-surface aquifer. Geophys Res Lett 6225(18):355–366. https://doi.org/10.1029/2004gl020661

Ghavanloo E, Daneshmand F, Rafiei M (2010) Vibration and instability analysis of carbon nanotubes conveying fluid and resting on a linear viscoelastic Winkler foundation. Phys E 42:2218–2224. https://doi.org/10.1016/j.physe.2010.04.024

Guo J, Luo B, Lu C, Lai J, Ren J (2017) Numerical investigation of hydraulic fracture propagation in a layered reservoir using the cohesive zone method. Eng Fract Mech. https://doi.org/10.1016/j.engfracmech.2017.10.013

Hu XJ, Li WP, Cao DT, Liu MC (2012) Index of multiple factors and expected height of fully mechanized water flowing fractured zone. J China Coal Soc 37:613–620(618)

Huang L, Hao H, Li X, Li J (2018a) Source identification of microseismic events in underground mines with interferometric imaging and cross wavelet transform. Tunn Undergr Space Technol 71:318–328. https://doi.org/10.1016/j.tust.2017.08.024

Huang L, Li J, Hao H, Li X (2018b) Micro-seismic event detection and location in underground mines by using convolutional neural networks (CNN) and deep learning. Tunn Undergr Space Technol 81:265–276. https://doi.org/10.1016/j.tust.2018.07.006

Jehring MM, Bareither CA (2016) Tailings composition effects on shear strength behavior of co-mixed mine waste rock and tailings. Acta Geotechnica 11(5):1147–1166. https://doi.org/10.1007/s11440-015-0429-1

Liu X, Tan Y, Ning J, Tian C, Wang J (2015) The Height of Water-Conducting Fractured Zones in Longwall Mining of Shallow Coal Seams. Geotech Geol Eng 33:693–700. https://doi.org/10.1007/s10706-015-9851-2

Palchik V (2003) Formation of fractured zones in overburden due to longwall mining. Environ Geol 44:28–38

Peng K, Li X-b, Wan C-c, Peng S-q, Zhao G-y (2012) Safe mining technology of undersea metal mine. Trans Nonferrous Metals Soc China 22:740–746. https://doi.org/10.1016/s1003-6326(11)61239-9

Sanshandao Gold Mine (2012) Sanshandao Gold Mine geological survey report (report). Sanshandao Gold Mine, China, Yantai

State Bureau of Coal Industry (2000) Regulations of buildings, water, rail way and main well lane leaving coal pillar and press coal mining. China Coal Industry Publishing House, China, Beijing

Sijing C (2009) Mine backfill mechanics Foundation, 2nd edn. Metallurgical industry press, China, Beijing

Wang S, Li X (2016) Dynamic distribution of longwall mining-induced voids in overlying strata of a coalbed. Int J Geomech 17:04016124

Wang JA, Shang XC, Ma HT (2008) Investigation of catastrophic ground collapse in Xingtai gypsum mines in China. Int J Rock Mech Min Sci 45:1480–1499. https://doi.org/10.1016/j.ijrmms.2008.02.012

Wang F, Tu S, Zhang C, Zhang Y, Bai Q (2016a) Evolution mechanism of water-flowing zones and control technology for longwall mining in shallow coal seams beneath gully topography. Environ Earth Sci. https://doi.org/10.1007/s12665-016-6121-4

Wang S, Li X, Wang D (2016b) Void fraction distribution in overburden disturbed by longwall mining of coal. Environ Earth Sci. https://doi.org/10.1007/s12665-015-4958-6

Wang G, Wu M, Wang R, Xu H, Song X (2017a) Height of the mining-induced fractured zone above a coal face. Eng Geol 216:140–152. https://doi.org/10.1016/j.enggeo.2016.11.024

Wang H, Zhang D, Wang X, Zhang W (2017b) Visual exploration of the spatiotemporal evolution law of overburden failure and mining-induced fractures: a case study of the Wangjialing coal mine in China. Minerals 7:35. https://doi.org/10.3390/min7030035

Wang S, Li X, Wang S (2017c) Separation and fracturing in overlying strata disturbed by longwall mining in a mineral deposit seam. Eng Geol 226:257–266. https://doi.org/10.1016/j.enggeo.2017.06.015

Wang S, Li X, Wang S (2018a) Three-dimensional mineral grade distribution modelling and longwall mining of an underground bauxite seam. Int J Rock Mech Min Sci 103:123–136

Wang S, Li X, Du K, Wang S, Tao M (2018b) Experimental study of the triaxial strength properties of hollow cylindrical granite specimens under coupled external and internal confining stresses. Rock Mech Rock Eng 51:2015–2031

Wang S, Li X, Du K, Wang S (2018c) Experimental investigation of hard rock fragmentation using a conical pick on true triaxial test apparatus. Tunn Undergr Space Technol 79:210–223

Xu N, Zhang J, Tian H et al (2016) Discrete element modeling of strata and surface movement induced by mining under open-pit final slope. Int J Rock Mech Min Sci 88:61–76. https://doi.org/10.1016/j.ijrmms.2016.07.006

Ye Q, Wang WJ, Wang G, Jia ZZ (2017) Numerical simulation on tendency mining fracture evolution characteristics of overlying strata and coal seams above working face with large inclination angle and mining depth. Arab J Geosci 10:82

Yin H, Wei J, Lefticariu L, Guo J, Xie D, Li Z, Zhao P (2016) Numerical simulation of water flow from the coal seam floor in a deep longwall mine in China. Mine Water Environ 35:243–252. https://doi.org/10.1007/s10230-016-0385-5

Zhang J, Peng S (2005) Water inrush and environmental impact of shallow seam mining. Environ Geol 48:1068–1076. https://doi.org/10.1007/s00254-005-0045-8

Zhang D, Fan G, Wang X (2012) Characteristics and stability of slope movement response to underground mining of shallow coal seams away from gullies. Int J Min Sci Technol 22:47–50. https://doi.org/10.1016/j.ijmst.2011.06.005

Zhang C, Mitra R, Oh J, Canbulat I, Hebblewhite B (2017) Numerical analysis on mining-induced fracture development around river valleys. Int J Min Reclam Environ. https://doi.org/10.1080/17480930.2017.1293495

Zhao C, Bai B (2009) Soil mechanics principle (revised edition). Tsinghua University Press, Beijing

Zhao GY, Yan-Liang PY (2009) Study on the Safety Mining Technology of Seabed Hard Rock. China Saf Sci J 5:29